Precipitation of non-spherical particles in aluminium alloys Part I: generalization of the Kampmann-Wagner numerical model

Bjørn Holmedal[1], Elisa Osmundsen[1], Qiang Du[2*]

[1]Norwegian University of Science and Technology

[2]SINTEF Materials and Chemistry, Trondheim, Norway

* Corresponding author: qiang.du@sintef.no

Abstract

Particles precipitated during aging treatments often have non-spherical shapes, e.g. needles or plates, while in the classical Kampmann-Wagner Numerical (KWN) precipitation model it is assumed that the particles are of spherical shape. This model is here generalized resulting in two correction factors accounting for the effects induced by the particles' non-spherical shape on their growth kinetics. The first one is for the correction of the growth rate. It is derived from the approximate solution of the diffusion problem on spheroidal coordinate and verified by the three-dimensional numerical solutions for cuboid particles. The second factor is for the energetic correction due to the particle surface curvature. It is derived from chemical potential equality (or Gibbs energy minimization principle) at equilibrium for non-spherical particles and provides a correction factor for the Gibbs-Thomson effect. In the accompanying paper the two correction factors are implemented into a multi-component KWN modelling framework and the resulting improvements on the model's predictive power are demonstrated.

1. Introduction

Precipitation kinetics in the age hardenable aluminum alloys are quite complex. The formation of an equilibrium precipitate phase is preceded by a series of metastable non-

spherical ones due to their ease of nucleation and anisotropies in their misfit strain energy, interfacial energy and attachment kinetics. Examples includes needle β" precipitates in Al-Mg-Si [1], plate θ' precipitates in Al-Cu [2], platelet η' precipitates in Al-Zn-Mg [3], and lath S-family of precipitates in Al-Cu-Mg alloys [4]. Non-spherical precipitates are beneficial as they contribute to larger peak hardness via their effective blockage to dislocation motion [5]. Various shaped precipitates have different growth kinetics. It is the aim of this paper to model the effects of particle shape on precipitate kinetics to improve the predictive power of the existing precipitation modeling tools for industrial aluminum alloys. It will be assumed that precipitate growth is fully diffusion controlled.

Continuing research effort has been made to develop general and composition-dependent models for the aging treatment of commercial aluminum alloys to predict the evolution of precipitate fraction, size, number density, morphology, and solid solution solute level. The reported approaches for this purpose fall into two categories: direct detailed approaches [6, 7] and physically based internal state variable approaches [8, 9]. The former is represented by the phase field method or Finite Difference Method and excels in providing detailed descriptions of nucleation, growth and coarsening. The latter, represented by Kampmann-Wagner Numerical (KWN) model [9], prevails in handling precipitation involving multi-scale transportation phenomena (e.g., concurrent nucleation, growth and coarsening of an ensemble of precipitates, precipitation in matrix with an uneven compositional profile etc.). Successful examples of the state variable approaches include modeling the formation of dispersoids free zone during homogenization heat treatment of AA3xxx series aluminum alloys [10], the up-quenching of AA6060 aluminum alloys [11, 12], and the computation of time-temperature-precipitation diagrams of industrial alloys [13], to name a few among many examples reported in the literature. The approaches in the two categories are complementary to each other as evidenced by the way the KWN model is generalized in this paper. On one hand, the detailed approaches could be used as computational experiments to verify/guide the

internal state variable approaches. On the other hand, when it comes to the important applications to industrial problems, the latter approach is superior due to its ability to efficiently address the multi-scale and multi-parameter problem.

The KWN model, to be generalized in this paper, utilizes approximate solution of the diffusion equation individually for each precipitating particle and a mean field concept to treat particles interaction. The methodology of this type of approaches is that the continuous precipitate size distribution curve could be subdivided into size classes, each of which is associated with a number of identical precipitates. The temporal evolution of the size distribution is then tracked by following the size evolution of each discrete size class. Mathematically this corresponds to an ordinary differential equation for each particle size as a function of time. In some cases this differential equation can be regarded as the characteristic equation for a first order conservation equation and the theory can be formulated as an equivalent partial differential equation for the particle size distribution, i.e. an Eulerian instead of Lagrangian description in terms of particle radius and time.

The classical KWN model employs the spherical precipitate shape assumption. The main requirement to generalize the model to cases of non-spherical precipitates is the solution of the corresponding diffusion problem, i.e. calculating the compositional profile surrounding a non-spherical particle embedded in a matrix of solid solution in order to calculate the growth rate of the particles. Assuming fixed concentrations at the particle interface and in the matrix far away, analytical time dependent solutions have been reported for ellipsoids and paraboloids by Ham [14] and by Horvay and Cahn [15]. These solutions are all shape-preserving similarity solutions, i.e. the particle aspect ratios remain constant, even when the diffusion properties are anisotropic. Reasonable simplified approximations to the growth rate can be obtained assuming quasi-steady state, where the particle radius is updated by the solutions of the Laplace's equation [16]. The validity of this approximation is discussed in [17, 18], where it is referred to as "invariant field approximations". A review of a variety of

approximations for needles and platelets can be found in the recent book by Aaronson et al. [19].

The diffusion solutions required for invariant field solutions have been provided for cases of spheroids, including special cases of elliptical platelets and infinitely long cylinders, by Ham in [20, 21], corresponding to the shape invariant time-dependent solutions [14, 15]. Ferrante and Doherty [22] utilized a simplification of Ham's solution for the growth and coarsening of very thin plate-shaped precipitates in Al-Ag alloys, with width to thickness aspect ratio of more than 100. They also estimated a solution for smaller aspect ratios based on a rough curve fitting involving numerical solutions required as a part of the analytical time dependent solution. Liu et al. [23] applied their approximation for the case of plate shaped precipitates in an Al-Mg-Cu alloy, which has smaller aspect ratios. Furthermore they adapted this simplified diffusion solution to cover the case of needle-shaped particles precipitated in Al-Mg-Si alloys. However, they made a mistake when directly transferring the small aspect ratio simplification to the case of needles, as it turns out that it is only valid for the case of plates. This mistake was inherited later by Song [24] and by Bahrami et al. [25], when considering needle shaped precipitates in Al-Mg-Si alloys. In addition the assumption in [25] yields a growth rate of only about 1/20 of the spherical precipitate's volumetric growth rate (with the invariant field approximation). It should be noted they reported that the growth rate decreases with increasing aspect ratio of needles of equal volume.

In their recent work Bardel et al. [26] applied a variant of the Zener-Hillert approximation to the diffusion solution for needle-shaped precipitates during non-isothermal treatment of an AA6061 aluminum alloy. Details about their diffusion solution is not provided, but it seems to be based on the approach from [27] applying a diffusion length scale proportional to the tip radius of the needle combined with the assumption of particle shape invariance. Bardel et al also predicted a decaying growth rate with increased aspect ratio.

Kozeschnik et al. [28] considered the effect of the aspect ratio on growth kinetics in their thermodynamic variational modelling framework. In their simplified approach the local equilibrium at the particle surface is not enforced. A shape factor for diffusion is introduced based on a comparison of the spherical particle solution to stationary finite-element simulations for precipitates with geometrical shape as cylinders. Their simulations apply boundary conditions corresponding to a flux through the particle surface being in total equal to that of a spherical particle of the same volume, i.e. equal growth rate of the particle volume (i.e equivalent radius). Still the shape change and the redistribution of the diffusional field somehow modify the dissipation of Gibbs energy and its extremum. When considering the fully diffusion-controlled growth mode, the disc shaped precipitates is predicted to grow considerable faster than spherical particles and similar with an aspect ratio around unity. However, the long cylinder shaped precipitates are predicted to grow slower than spherical particles of equal volume. Note that the assumption of equal flux into the particle implies a different solute concentration at the particle surface than for the reference spherical particle. This will alter the local equilibrium between the chemical potentials, but this never enters their simplified variational approach.

Very surprisingly, most of the recent investigations mentioned above reported a negative dependence of the volumetric growth rate on aspect ratio. In contradiction Ham’s early works [20, 21] corresponds to a positive influence. In this paper, Ham's original treatment is extended and verified by a detailed 3D numerical solution to model precipitation of arbitrarily-shaped particles. Furthermore, the Gibbs-Thomson effect for various particle shapes, which is the other important requirement to generalize the KWN model, is derived. The two corrections factors will be outlined for the case of binary alloys, but can easily be generalized to multi-component system in the same way as reported in [29].

The paper is organized as follows. Section 2 describes the derivation of the two correction factors for needle shaped particles. A discussion is presented in Section 3, and the last section is for conclusions.

2. Model description

In this section, two correction factors, i.e. one for growth rate and one for particle surface curvature influence, are derived to account for the effects induced by particles' non-spherical shape. The other ingredients of the KWN model are not altered, i.e. mass balance and nucleation. They will be shown here for the case of binary alloys, but it can easily be generalized to multi-component.

2.1 The growth rate correction

For fully diffusion-controlled growth, the key in deriving rate equation is to calculate the diffusional flux of solute to the migrating matrix-precipitate interface. We have adopted the commonly used simplifying assumption that the diffusion problem can be treated as quasi-static. It implies the separate solution of the stationary diffusion equation for each particle embedded in the matrix without considering direct interactions with the diffusion fields of its neighbouring particles. The concentration at the particle surface and the concentration in the matrix far away from the particle are assumed to change slowly, so that the steady solution can be applied but with updated values of the time dependent boundary conditions. The diffusion problem for the concentration c of an element in solid solution can then be written:

$$\nabla^2 c = 0 \tag{1}$$

Here $c = c_m$ in the matrix far away from the particle, and $c = c_i$ at the particle interface. The flux into the particle according to Ficks' first law can be integrated to calculate the flux of

solute through the precipitate interface. Utilizing the scaling properties of Eq.(1) the solution can be expressed for general particle shapes as

$$I = \iint\limits_{\substack{\text{particle} \\ \text{interface}}} \frac{\partial c}{\partial n} dS = 4\pi D(c_m - c_i) R f \tag{2}$$

Here n is the outward normal direction to the particle surface segment dS. Furthermore, D is the diffusion coefficient, R is the radius of an equivalent sphere, whose volume is identical to the particle volume, and f is a correction factor depending on the particle shape. The scaling factor 4π is chosen so that $f = 1$ for the special case of a spherical particle shape.

The flux balance gives

$$Idt = \left(c_i - c_p\right) dV \tag{3}$$

where c_p is the solute concentration (per volume) in the particle. It follows from Eq. (3) that the growth rate of the radius of an equivalent spherical particle, whose volume is equal to the considered particle, and by applying Eq. (1), that

$$\frac{dR}{dt} = f \frac{\left(c_m - c_i\right)}{\left(c_p - c_i\right)} \frac{D}{R} \tag{4}$$

Equation (2) defines the first shape correction factor, f. This factor can be obtained once the diffusion solution is available, as will be shown for the following two complementary methods.

2.1.1 Correction factor from the analytical diffusion solutions for spheroids

For the sake of clarity Ham's treatment will be briefly rewritten to appropriate expressions to be used here. The surface of a prolate spheroid with length of L and radius of r_0 is given by

$$\frac{x^2+y^2}{r_0^2}+\frac{4z^2}{L^2}=1 \tag{5}$$

Here $L>2r_0$. The aspect ratio is defined as $\alpha=L/(2r_0)$. The volume, V, of the prolate spheroid is

$$V=\frac{4\pi}{6}r_0^2L \tag{6}$$

The eccentricity e and surface area, S are given by

$$e=\sqrt{1-\frac{4r_0^{\,2}}{L^2}}=\sqrt{1-\frac{1}{\alpha^2}} \tag{7}$$

$$S=2\pi r_0^2\left(1+\frac{L}{2r_0e}\sin^{-1}e\right) \tag{8}$$

The radius, R, of an equivalent sphere, whose volume is identical to the spheroid equals

$$R=\sqrt[3]{\frac{Lr_0^{\,2}}{2}} \tag{9}$$

Prolate spheroidal coordinates are to be employed in our analysis. The spheroidal coordinates can be transformed from Cartesian coordinates by

$$\xi=\frac{1}{\sqrt{L^2-4r_0^2}}\left(\sqrt{x^2+y^2+\left(z+\frac{1}{2}\sqrt{L^2-4r_0^2}\right)^2}+\sqrt{x^2+y^2+\left(z-\frac{1}{2}\sqrt{L^2-4r_0^2}\right)^2}\right) \tag{10}$$

$$\eta=\frac{1}{\sqrt{L^2-4r_0^2}}\left(\sqrt{x^2+y^2+\left(z+\frac{1}{2}\sqrt{L^2-4r_0^2}\right)^2}-\sqrt{x^2+y^2+\left(z-\frac{1}{2}\sqrt{L^2-4r_0^2}\right)^2}\right) \tag{11}$$

$$\phi=\arctan\left(\frac{y}{x}\right) \tag{12}$$

An analytical solution, which only depends on ξ, can be derived, for which ∇^2 becomes $\frac{d}{dz}((\xi^2-1)\frac{d}{dz})$. The surface of the prolate spheroid is obtained at $\xi = \xi_0 = L^2/(L^2-4r_0^2)$. In the limit of large values of ξ the coordinates become more and more spherical, i.e. $\xi \to \sqrt{x^2+y^2+z^2}$ for large radiuses.

Eq.(1) is complemented with the following boundary conditions:

$$c = c_m \text{ for } \xi \to \infty \text{, i.e. on a sphere of infinite radius} \tag{13}$$

$$c = c_i \text{ on the prolate surface, i.e. } \xi = \xi_0 = L/\sqrt{L^2-4r_0^2} \tag{14}$$

The analytical solution has been proposed in [21], according to which the compositional profiles surrounding the growing spheroid with the dimension of ξ_0 is described by:

$$c(\xi) = c_m + (c_i - c_m)\left(1 - \frac{\ln\left((\xi+1)(\xi_0-1)\right) - \ln\left((\xi-1)(\xi_0+1)\right)}{\ln(\xi_0-1) - \ln(\xi_0+1)}\right) \tag{15}$$

In the limit where $L = 2r_0$ Eq. (15) degenerates smoothly to the special case of the spherical precipitate, for which

$$c = c_m + (c_i - c_m)\frac{r_0}{r} \tag{16}$$

Here $r = \sqrt{x^2+y^2+z^2}$. From the compositional profile expressed by Eq. (15), the flux according to Ficks' first law can be integrated to calculate the flux of solute through the precipitate interface:

$$I = \frac{4\pi D(c_i - c_m)Le}{\ln(1+e) - \ln(1-e)} = f(\alpha)4\pi D(c_i - c_m)R \tag{17}$$

$$f(\alpha)=\frac{2\sqrt{\alpha^2-1}}{\sqrt[3]{\alpha}\ln\left(2\alpha^2+2\alpha\sqrt{\alpha^2-1}-1\right)} \tag{18}$$

For the special limit of spheres, i.e. with $\alpha=1$, the shape factor $f(\alpha)$ degenerates smoothly to $f(1)=1$. Eq. (18) is monotonically increasing, and within this fully diffusion-controlled growth scenario, where the growth rate is proposal to the solute current, the spherical particle has the slowest growth rate. As the shape becomes more non-spherical (i.e., with the increase of aspect ratio), the growth becomes faster. As shown by the $f(\alpha)$ curve in in Fig. 1 when the aspect ratio is larger than 10, the needle shape has a growth rate more than 50% faster than the spherical particles.

2.1.2 Correction factor from numerical diffusion solution for cuboids

A cuboid needle shaped particle of width w and length $l=\beta w$ (β is the aspect ratio) is considered. The radius of its volume-equivalent sphere can be expressed as:

$$R=\sqrt[3]{\frac{3\beta}{4\pi}}w \tag{19}$$

The diffusion problem consists of solving Eq.(1) with appropriate boundary conditions, i.e., $c=c_i$ at the particle surface and $c=c_m$ infinitely far away from the particle. Due to the symmetry, only one eighth of the particle needs to be calculated. However the only ways this limit can be reached and still fulfil Eq.(1), is by c approaching a constant value on a sphere in the limit of an infinitely large radius. At a finite but large distance from the particle the solution can be written:

$$c=c_m+\frac{I}{4\pi\sqrt{x^2+y^2+z^2}} \tag{20}$$

Here I is the solute flux in through a closed surface Γ surrounding the particle

$$I = \int_{\Gamma} \frac{\partial c}{\partial n} d\Gamma \tag{21}$$

Here n is the normal direction out of the infinitesimal surface element $d\Gamma$.

A numerical solution can be obtained on a finite domain by introducing the following coordinate transformation:

$$\hat{x} = \frac{w}{x+w}, \quad \hat{y} = \frac{w}{y+w}, \quad \hat{z} = \frac{w}{x+\beta w} \tag{22}$$

Here it is convenient to introduce the dimensionless concentration:

$$\varphi = \frac{c - c_m}{c_i - c_m} \tag{23}$$

Eq.(1) can now be written as

$$\hat{x}^3 \left(\hat{x} \frac{\partial^2 \varphi}{\partial \hat{x}^2} + \frac{\partial \varphi}{\partial \hat{x}} \right) + \hat{y}^3 \left(\hat{y} \frac{\partial^2 \varphi}{\partial \hat{y}^2} + \frac{\partial \varphi}{\partial \hat{y}} \right) + \hat{z}^3 \left(\hat{z} \frac{\partial^2 \varphi}{\partial \hat{z}^2} + \frac{\partial \varphi}{\partial \hat{z}} \right) = 0 \tag{24}$$

At the particle surface the boundary conditions are

$$\varphi = 1 \text{ at } \begin{cases} \hat{x} = \frac{1}{2}, \ \hat{y} \le 1 \text{ and } \frac{1}{2\alpha} \le \hat{z} \le \frac{1}{\alpha} \\ \hat{y} = \frac{1}{2}, \ \frac{1}{2} \le \hat{x} \le 1 \text{ and } \frac{1}{2\alpha} \le \hat{z} \le \frac{1}{\alpha} \\ \hat{z} = \frac{1}{2\alpha}, \ \frac{1}{2} \le \hat{x}, \ \hat{y} \le 1 \end{cases} \tag{25}$$

At the symmetry surfaces

$$\left. \frac{\partial \varphi}{\partial \hat{x}} \right|_{\hat{x}=1} = 0 \text{ when either } 0 \le \hat{y} \le \frac{1}{2} \text{ or } 0 \le \hat{z} \le \frac{1}{2\beta} \tag{26}$$

$$\left.\frac{\partial\varphi}{\partial\hat{y}}\right|_{\hat{y}=1} = 0 \text{ when either } 0 \le \hat{x} \le \frac{1}{2} \text{ or } 0 \le \hat{z} \le \frac{1}{2\beta} \tag{27}$$

$$\left.\frac{\partial\varphi}{\partial\hat{y}}\right|_{\hat{z}=\frac{1}{\beta}} = 0 \text{ when either } 0 \le \hat{x} \le \frac{1}{2} \text{ or } 0 \le \hat{y} \le \frac{1}{2} \tag{28}$$

A Dirichlet condition cannot by applied at infinity as the solution unfortunately degenerates singularly on a cuboid domain, i.e. the solution has to become constant on a sphere as it fades out (this is an odd-dimensional property of the Laplace equation and is also the case for the analytical spheroid solutions above). To overcome this limitation of the Cartesian grid, the analytical asymptotic solution is prescribed at the first node away from this limit, formally defined by a small value δ for each transformed direction as follows:

$$\varphi = \frac{I}{4\pi\sqrt{\hat{x}^{-2}+\hat{y}^{-2}+\hat{z}^{-2}}} \text{ when } \begin{cases} \hat{x} = \delta,\ 0 \le \hat{y} \le 1, 0 \le \hat{z} \le \dfrac{1}{\beta} \\ \hat{y} = \delta, 0 \le \hat{x} \le 1,\ 0 \le \hat{z} \le \dfrac{1}{\beta} \\ \hat{z} = \dfrac{\delta}{2\beta},\ 0 \le \hat{x},\ \hat{y} \le 1 \end{cases} \tag{29}$$

Here the non-dimensional calculated solute current is

$$\hat{I} = 8\left(\int_{\frac{1}{2}}^{1}\int_{\frac{1}{2}}^{1} \frac{\hat{z}^2}{\hat{x}^2\hat{y}^2}\left.\frac{\partial\varphi}{\partial\hat{z}}\right|_{\hat{z}=\frac{1}{2\alpha}} d\hat{x}d\hat{y} + \int_{\frac{1}{2}}^{1}\int_{\frac{1}{2\beta}}^{\frac{1}{\beta}} \frac{\hat{x}^2}{\hat{y}^2\hat{z}^2}\left.\frac{\partial\varphi}{\partial\hat{x}}\right|_{\hat{x}=\frac{1}{2}} d\hat{y}d\hat{z} + \int_{\frac{1}{2}}^{1}\int_{\frac{1}{2\beta}}^{\frac{1}{\beta}} \frac{\hat{y}^2}{\hat{x}^2\hat{z}^2}\left.\frac{\partial\varphi}{\partial\hat{y}}\right|_{\hat{y}=\frac{1}{2}} d\hat{x}d\hat{z} \right) \tag{30}$$

Finally the solute current can be expressed

$$I = wD\left(c_i - c_m\right)\hat{I} \tag{31}$$

Here $\hat{I}$ is obtained from the simulation for a given aspect ratio β. By including this integral in the boundary equation Eq. (24) could be solved by iterative techniques. Note that $\hat{I}$ depends only on the particle shape, not on its volume. By comparison to Eq. (2) and use of

Eq (19) the shape factor for cuboids can be found from the numerical result as a function of the aspect ratio

$$f = \frac{\hat{I}}{\left(48\pi^2\beta\right)^{\frac{1}{3}}} \tag{32}$$

For a slowly changing aspect ratio (in terms of no modification of the quasi steady diffusion solution (31)) Eq. (4) can alternatively be rewritten in terms of w or l.

$$\frac{dw}{dt} = \frac{1}{\beta^{\frac{2}{3}}\left(1+\frac{w}{3\beta}\frac{d\beta}{dw}\right)}\frac{\kappa f D}{w} \tag{33}$$

$$\frac{dl}{dt} = \frac{\beta^{\frac{4}{3}}}{\left(1-\frac{2l}{3\beta}\frac{d\beta}{dl}\right)}\frac{\kappa f D}{l} \tag{34}$$

$$\kappa = \left(\frac{4\pi}{3}\right)^{\frac{2}{3}}\frac{\left(c_m - c_i\right)}{\left(c_p - c_i\right)} \tag{35}$$

Note that here the gradual change of the aspect ratio is accounted for. Similar equations can easily be derived for the major axes of spheroids.

The shape function $f(\beta)$ can be found for various aspect ratios by fully three-dimensional numerical simulations. A second order central difference finite difference discretization of Eqns. (24)-(30) was made. Discretizing the computational domain by 120^3 points was found to be sufficient for a numerical accuracy of $\hat{I}$ of about 2%, estimated based on comparison to a few simulations with 150^3 points. An example of the type of mesh used is shown in Fig 2. The resulting equation system was solved iteratively by a line iterative method utilizing the efficient Thomas algorithm for linearization into tridiagonal matrices during iterations. The dependency on the aspect ratio is shown by the $f(\beta)$ curve in Fig. 1. In the same figure the relation (18) for the case of spheroids is also shown. A good fit to the cuboid shape factor, i.e.

Eq. (32), with less than 1% error as compared to the numerical results, can be found by the formula

$$f(\beta) = 0.1\exp\left(-0.091\left(\beta - 1\right)\right) + \frac{1.736\sqrt{\beta^2 - 1}}{\sqrt[3]{\beta}\ln\left(2\beta^2 + 2\beta\sqrt{\beta^2 - 1} - 1\right)} \tag{36}$$

2.2 The Gibbs-Thomson effect

For a spherical particle precipitated in a dilute binary solid solution matrix the curvature is the same everywhere on the particle surface. It is well documented, e.g. [30], that according to chemical potential equality, or Gibbs energy minimization principle, at equilibrium the Gibbs-Thomson effect in this simplified case would modify the interfacial phase composition via:

$$c_i = c_m \exp\left(\frac{2\sigma \mathrm{v}_m^{\beta}}{RkT}\right) \tag{37}$$

Here σ the interfacial energy, v_m^{β} the phase molar volume and kT is the product of the Boltzmann constant and temperature.

The Gibbs energy minimization principle also applies for non-spherical particles. However for a non-spherical particle the Gibbs-Thomson effect would modify the interfacial phase compositions along its interface to various extents due to the variation of the local mean curvature. For example for prolate spheroids, this local mean curvature is given by:

$$\gamma = \frac{\frac{L}{2}\left(2{r_0}^2 + \left(\frac{L^2}{4} - {r_0}^2\right)cos^2\phi\right)}{2r_0\left({r_0}^2 + \left(\frac{L^2}{4} - {r_0}^2\right)cos^2\phi\right)^{3/2}} \quad , -\frac{\pi}{2} < \phi < \frac{\pi}{2} \tag{38}$$

Obviously the local curvature depends on the azimuth ϕ. The detailed treatment of the variation of solute concentration along a needle-shaped particle surface is a difficult task. Such an approach is required to predict the shape change of the particle. However, in many applications the shape can be prescribed from experimental observations. In addition the shape change depends on other factors that are neglected in a KWN model, e.g. the anisotropy of the particle surface energy, deviations from perfect diffusion controlled growth. It is likely that the shape predictions otherwise would be wrong without use of more detailed, costly model approaches.

To simplify the mathematical treatment of the Gibbs-Thomson effect it is here assumed that precipitates take a prescribed shape and aspect ratio during their growth. Furthermore it is assumed that aspect ratio changes sufficiently slowly for considering it quasi constant in the treatment of the Gibbs-Thomson effect. Together with the Gibbs energy minimization principle these assumptions allow a straightforward extension of Eq. (9) to non-spherical shaped particles. For the sake of simplicity ordered precipitates in a binary alloy will be considered.

Due to the presence of the interface (of area S^β), the Gibbs energy of an ordered β phase particle of n^β atoms is:

$$G^\beta = n^\beta \mu^\beta + \sigma S^\beta \tag{39}$$

Here μ_m^β is the free energy per atom of component β (i.e. the chemical potential). atoms in the β phase is linked with the volume of the particle, V^β, by

$$V^\beta = n^\beta \mathrm{v}_m^\beta \tag{40}$$

Here v_m^β is the molar volume of the β phase. Taking into account the Gibbs-Thomson effect, the chemical potential of the alloying component in the precipitating particle is

$$\frac{\partial G^\beta}{\partial n^\beta} = \mu^\beta + \sigma \frac{\partial S^\beta}{\partial n^\beta} \tag{41}$$

For a prescribed shape the surface area of the particle is related to its volume

$$\frac{\partial G^\beta}{\partial n^\beta} = \mu^\beta + \sigma \frac{dS^\beta}{dV^\beta} \mathrm{v}_m^\beta = \mu^\beta + \frac{2g\sigma \mathrm{v}_m^\beta}{R} \tag{42}$$

The second shape factor g is here introduced as

$$g = \tfrac{1}{2} R \frac{dS^\beta}{dV^\beta} = \frac{1}{8\pi R} \frac{dS^\beta}{dR} \tag{43}$$

This factor is scaled so that $g = 1$ for a spherical particle.

The simplified Gibbs-Thomson effect for dilute binary alloys can be derived from Eq. (42) as explained in [30], and the interfacial phase composition for non-spherical particles can then be expressed

$$c_i = c_m \exp\left(\frac{2g\sigma \mathrm{v}_m^\beta}{RkT} \right) \tag{44}$$

The difference from the spherical shape in Eq. (37) is captured by the shape factor g. The use of the shape factor can be generalized to more complex cases of multi-component alloys.

For prolate spheroids with aspect ratio α the shape factor g equals:

$$g(\alpha) = \frac{1}{2\alpha^{\frac{2}{3}}} \left(1 + \frac{\alpha^2}{\sqrt{\alpha^2 - 1}} \sin^{-1}\left(\frac{\sqrt{\alpha^2 - 1}}{\alpha} \right) \right) \tag{45}$$

For the case of a cuboid particle with aspect ratio β the surface area equals $S^{\beta} = (4\beta + 2)w^2$ and by the use of Eq. (43) the second shape factor can be derived as

$$g(\beta) = \frac{(2\beta + 1)}{2\pi}\left(\frac{4\pi}{3\beta}\right)^{\frac{2}{3}} \tag{46}$$

The shape factor g, as predicted by Eqs. (45) and (46), is plotted in Fig. 2. The Gibbs-Thomson effect increases with increased aspect ratio.

3. Discussion

Two factors that depend only on the particle aspect ratio are introduced to generalize the KWN model. The first factor f, numerically verified by a detailed numerical approach, can be regarded as a modification of the volume equivalent spherical radius for the diffusion properties, i.e., the radius R/f corresponds to the equivalent radius of a spherical particle with equal diffusional flux into the particle as for the considered particle shape. Our two complementary treatments, i.e., Eq. (18) and Eq. (36), yield the positive dependence as shown in Fig. 1 in a convincing manner. The second factor g can be regarded as a modification of the equivalent radius when accounting for the energetic cost of creating new particle interface, i.e. the radius R/g corresponds to the equivalent radius of a spherical particle with equal cost as the considered particle in terms of creating new interfaces during growth.

If the particle shape remains unchanged during the heat treatment the introduction of the two correction factors is in practice equivalent to a modification of the diffusivity D and of the surface energy σ. Experimentally these two parameters are difficult to measure and the two factors clarify some of uncertainties in the measurement. It represents a reinterpretation of the application of an equivalent radius and justifies the use of the spherical KWN approach with

slightly adjusted parameters. Furthermore, it follows that there is no computational cost of this generalization, and it can directly be incorporated into existing KWN modelling framework as demonstrated in the accompanying paper.

In many cases the shape changes of the particles have been experimentally observed. For example nearly cuboid needle shaped precipitates in Al-Mg-Si alloys remain cuboid shape but their aspect ratio increases during aging treatment. Such a shape change will also slightly modify the diffusion solution, and if it occurs slowly, it can be treated by updating the shape parameters in the diffusion solution. In these cases the gradual change of the aspect ratio can be prescribed, say as a function of time or as a function of the equivalent radius. This is verified via a detailed experimental characterization in the accompanying paper.

It is also worth discussing in details how the proposed diffusion correction factor revise the ones reported in the literature [23, 25, 26, 28]. We summarize Shape factors f based on reported diffusion solutions as follows:

$$f=\left(\frac{3}{2}\right)^{\frac{2}{3}}\frac{2}{9\pi\alpha^{\frac{1}{3}}}\ ,\ \text{Bahrami et al. [25]} \tag{47}$$

$$f=\left(\frac{3}{2}\right)^{\frac{2}{3}}\frac{4}{3\alpha^{\frac{1}{3}}}\ ,\ \text{Liu et al. [23]} \tag{48}$$

$$f=\frac{3(6-2\alpha)^{\frac{2}{3}}}{32\alpha}\ ,\ \text{Bardel et al. [26]} \tag{49}$$

The model by Kozeschnick et al. [28] is based on a different framework where the shape factor f could not be described by a simple expression. Two things are noted from these results. Firstly the shape factors, in particular of [25] but also for [26] are considerable smaller than unity for the case of $\alpha=1$, i.e., the reported models do not degenerates to the spherical one when $\alpha=1$. Secondly, the growth rates predicted by these solutions for a needle of an aspect ratio of 25 are an order of magnitude slower than for the solutions

obtained by the proposed model, and also as compared to the equivalent radius approaches keeping $f = 1$, e.g. Myhr et al. [11].

Finally some words on the restrictions and future prospective of the generalized model. In the generalization the shape change has to be dealt with. When spherical particles grow in an isotropic matrix their shape remains spherical and the local equilibrium can be maintained everywhere at their surfaces. For the more general shapes to remain shape-preserved (i.e., aspect ratio being constant), the relative ratio of the flux between any two directions has to remain constant. For the cuboid particle this means that the dimensionless flux has to be constant on each of its flat sides, but not equal for orthogonal sides. This corresponds to prescribing the derivative of the solute concentration instead of the solute concentration itself. It is likely, but not obvious, that this also corresponds to a shape preserving time dependent solution. In the invariant field approximation the result will be a solute concentration variation along the particle surface. Since the cuboid needle has flat surfaces this is however approximately the case for large portions of the surfaces.

Cuboid particles have corners and edges. Their surface is not increased by the local curvature, but by the formation of new side wall area by that one of its edges is moving laterally as a consequence of that the opposing side grows normally. This will obviously increase the Gibbs free energy, but only very locally near edges, where the curvature is infinitely sharp. It seems reasonable to handle this by considering the Gibbs energy of the entire particle, so that a Gibbs-Thomson limitation is imposed even though the side walls are straight. Of course this means that the growth must be constrained and not entirely diffusion controlled. However, assuming the concentration is not varying too much along the particle surface, the approximation of a constant solute concentration at the particle surface can be justified. Very detailed simulations and dedicated experiments might shed light on the quality and deeper understanding of this approximation in the future.

4. Summary and conclusions

Two simple correction factors have been proposed to account for the effects induced by the precipitating particle's needle shape on their growth kinetics. The two factors generalize the KWN model and enable the prediction of the precipitation kinetics of non-spherical particles. To obtain the first factor, the steady state diffusion problem has been solved for the particle shape of interest based on two complementary treatments, i.e., an approximate solution of the diffusion problem on spheroidal coordinate and a three-dimensional numerical solution for cuboid particles. The second factor is for Gibbs-Thomson effect. It is derived from the Gibbs energy minimization principle for a non-spherical particle. Examples are provided for prolate spheroids and for cuboid needles. Other shapes can be calculated once and for all following the methodology outlined here. The two corrections factors will be applied in the accompanying paper to predict the precipitation kinetics during aging treatment of an Al-Mg-Si alloy.

References

[1] C.D. Marioara, S.J. Andersen, J. Jansen, H.W. Zandbergen. The influence of temperature and storage time at RT on nucleation of the beta " phase in a 6082 Al-Mg-Si alloy, Acta Mater 51 (2003) 789-796.

[2] A. Biswas, D.J. Siegel, C. Wolverton, D.N. Seidman. Precipitates in Al-Cu alloys revisited: Atom-probe tomographic experiments and first-principles calculations of compositional evolution and interfacial segregation, Acta Mater 59 (2011) 6187-6204.

[3] G. Sha, A. Cerezo. Early-stage precipitation in Al-Zn-Mg-Cu alloy (7050), Acta Mater 52 (2004) 4503-4516.

[4] Z. Chen, S. Li. Reinterpretation of precipitation behavior in an aged AlMgCu alloy, J Mater Sci 49 (2014) 7659-7668.

[5] P.M. Kelly. Effect of Particle Shape on Dispersion Hardening, Scripta Metall Mater 6 (1972) 647-656.

[6] B. Nestler, A. Choudhury. Phase-field modeling of multi-component systems, Curr Opin Solid St M 15 (2011) 93-105.

[7] G. Wang, D.S. Xu, N. Ma, N. Zhou, E.J. Payton, R. Yang, M.J. Mills, Y. Wang. Simulation study of effects of initial particle size distribution on dissolution, Acta Mater 57 (2009) 316-325.

[8] O. Grong, H.R. Shercliff. Microstructural modelling in metals processing, Prog Mater Sci 47 (2002) 163-282.

[9] R. Wagner, R. Kampmann. Homogeneous second phase precipitation. in: Cahn RW, Haasen P, Kramer EJ, (Eds.). Materials science and technology: a comprehensive treatment, vol. 5: Phase transformations in Materials. VCH, Weinheim, Germany, 1991. pp. 213-303.

[10] Q. Du, W.J. Poole, M.A. Wells, N.C. Parson. Microstructure evolution during homogenization of Al-Mn-Fe-Si alloys: Modeling and experimental results, Acta Mater 61 (2013) 4961-4973.
[11] O.R. Myhr, O. Grong. Modelling of non-isothermal transformations in alloys containing a particle distribution, Acta Mater 48 (2000) 1605-1615.
[12] O.R. Myhr, O. Grong, C. Schafer. An Extended Age Hardening Model for Al-Mg-Si Alloys Incorporating the Room Temperature Storage and Cold Deformation Process Stages, Metall Mater Trans A (Accepted for publication).
[13] J.D. Robson, M.J. Jones, P.B. Prangnell. Extension of the N-model to predict competing homogeneous and heterogeneous precipitation in Al-Sc alloys, Acta Mater 51 (2003) 1453-1468.
[14] F.S. Ham. Shape-preserving solutions of the time-dependent diffusion equation, Quarterly of Applied Mathematics 17 (1959) 137-145.
[15] G. Horvay, J.W. Cahn. Dendritic and Spheroidal Growth, Acta Metall Mater 9 (1961) 695-705.
[16] C. Wert, C. Zener. Interference of Growing Spherical Precipitate Particles, J Appl Phys 21 (1950) 5-8.
[17] S.R. Coriell, R.L. Parker. Stability of Shape of a Solid Cylinder Growing in a Diffusion Field, J Appl Phys 36 (1965) 632-637.
[18] H.B. Aaron, Fainstei.D, G.R. Kotler. Diffusion-Limited Phase Transformations - a Comparison and Critical Evaluation of Mathematical Approximations, J Appl Phys 41 (1970) 4404-&.
[19] H.I. Aaronson, M. Enomoto, J.K. Lee. Mechanisms of diffusional phase transformations in metals and alloys, CRC Press, Boca Raton, 2010.
[20] F.S. Ham. Theory of Diffusion-Limited Precipitation, J Phys Chem Solids 6 (1958) 335-351.
[21] F.S. Ham. Diffusion-Limited Growth of Precipitate Particles, J Appl Phys 30 (1959) 1518-1525.
[22] M. Ferrante, R.D. Doherty. Influence of Interfacial Properties on the Kinetics of Precipitation and Precipitate Coarsening in Aluminum-Silver Alloys, Acta Metall Mater 27 (1979) 1603-1614.
[23] G. Liu, G.J. Zhang, X.D. Ding, J. Sun, K.H. Chen. Modeling the strengthening response to aging process of heat-treatable aluminum alloys containing plate/disc- or rod/needle-shaped precipitates, Mat Sci Eng a-Struct 344 (2003) 113-124.
[24] M. Song. Modeling the hardness and yield strength evolutions of aluminum alloy with rod/needle-shaped precipitates, Mat Sci Eng a-Struct 443 (2007) 172-177.
[25] A. Bahrami, A. Miroux, J. Sietsma. An Age-Hardening Model for Al-Mg-Si Alloys Considering Needle-Shaped Precipitates, Metall Mater Trans A 43A (2012) 4445-4453.
[26] D. Bardel, M. Perez, D. Nelias, A. Deschamps, C.R. Hutchinson, D. Maisonnette, T. Chaise, J. Gamier, F. Bourlier. Coupled precipitation and yield strength modelling for non-isothermal treatments of a 6061 aluminium alloy, Acta Mater 62 (2014) 129-140.
[27] C. Zener. Kinetics of the Decomposition of Austenite, T Am I Min Met Eng 167 (1946) 550-595.
[28] E. Kozeschnik, J. Svoboda, F.D. Fischer. Shape factors in modeling of precipitation, Mat Sci Eng a-Struct 441 (2006) 68-72.
[29] Q. Du, W.J. Poole, M.A. Wells. A mathematical model coupled to CALPHAD to predict precipitation kinetics for multicomponent aluminum alloys, Acta Mater 60 (2012) 3830-3839.
[30] M. Perez. Gibbs-Thomson effects in phase transformations, Scripta Mater 52 (2005) 709-712.

Figure captions

Figure 1. The dependence of the diffusional correction factor f on the aspect ratio for cases of spheroid and cuboid particles.

Figure 2. Computational domain and grid used for finite difference solutions of Laplace's equation. A low resolution of 303 points is shown.

Figure 3. The dependence of the Gibbs-Thomson correction factor g on aspect ratios for cases of spheroid and cuboid particles

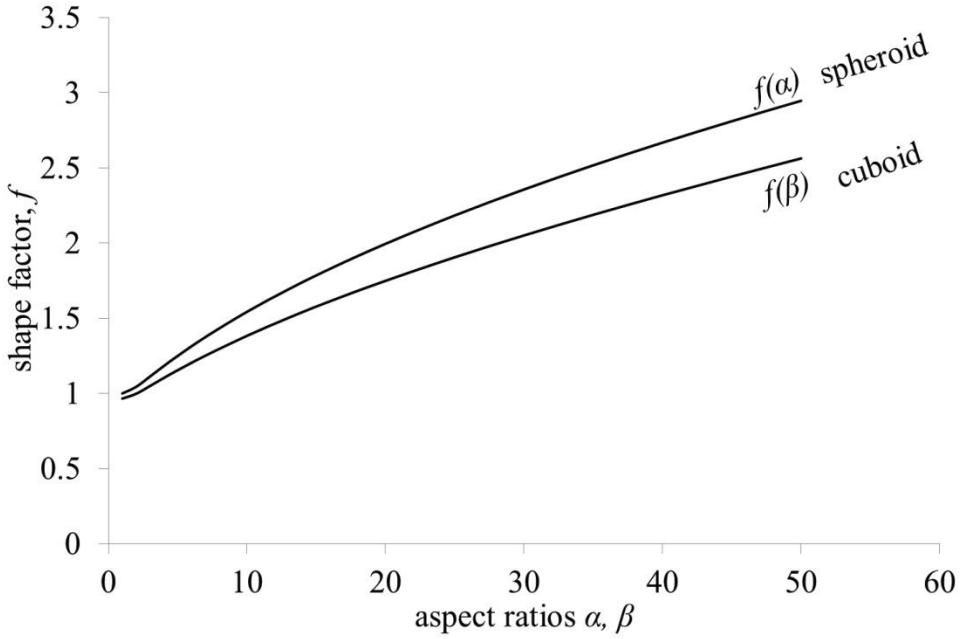

Figure 1. The dependence of the diffusional correction factor f on the aspect ratio for cases of spheroid and cuboid particles.

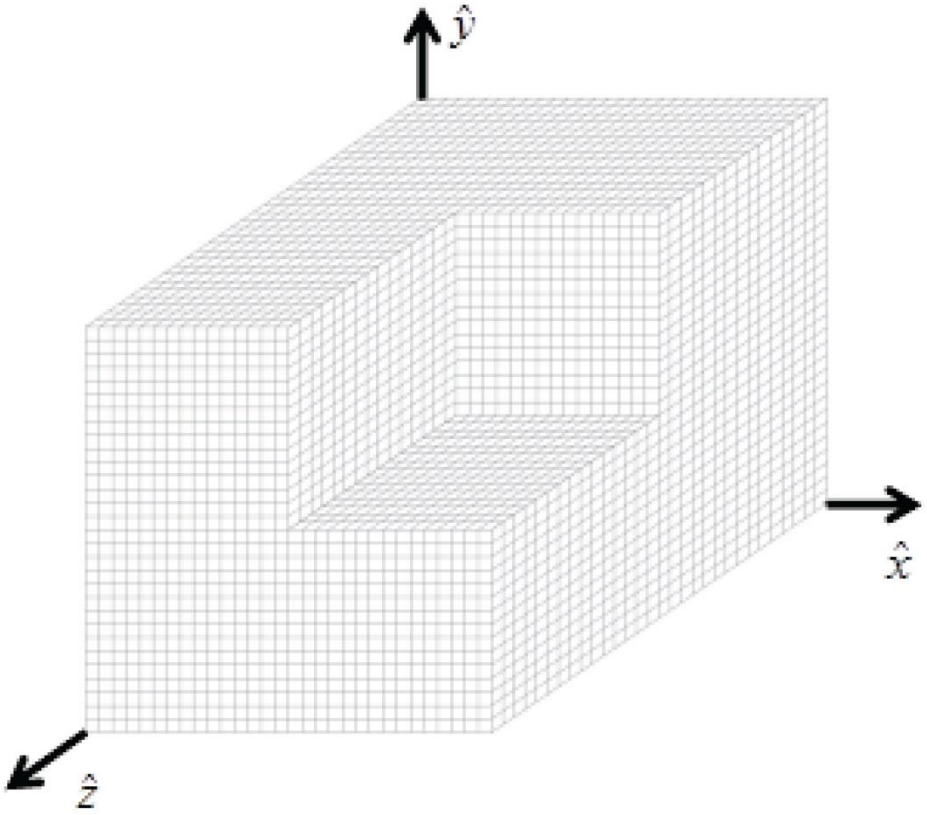

Figure 2. Computational domain and grid used for finite difference solutions of Laplace's equation. A low resolution of 303 points is shown.

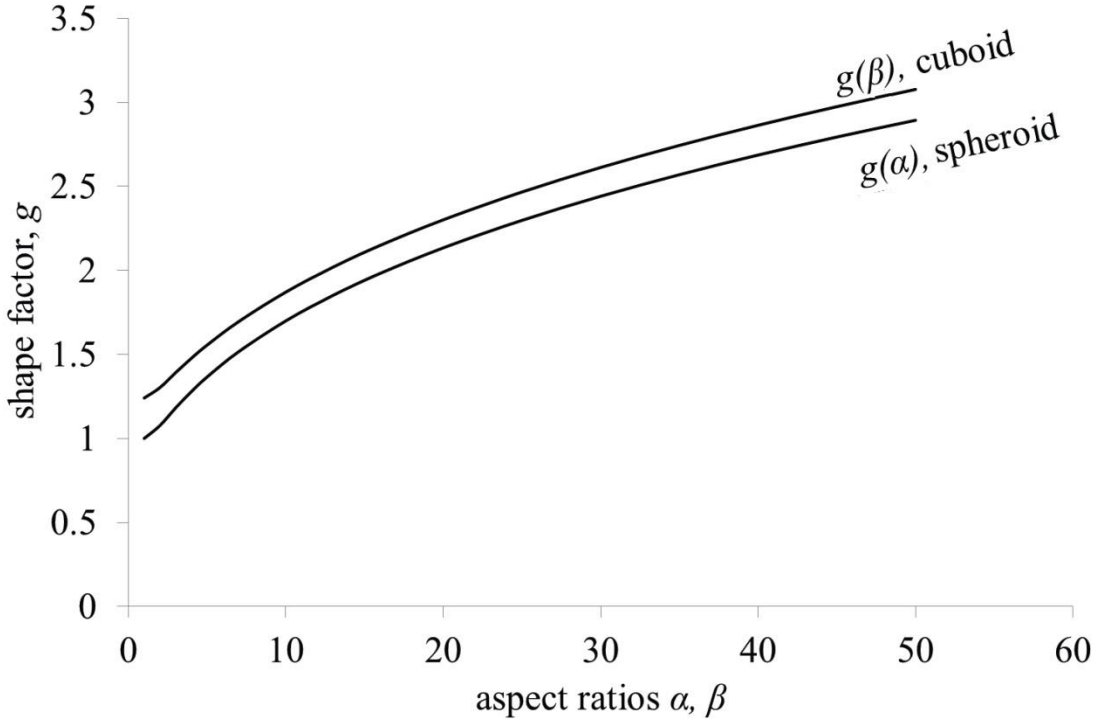

Figure 3. The dependence of the Gibbs-Thomson correction factor g on aspect ratios for cases of spheroid and cuboid particles